SGK regulates meiotic resumption in ovarian starfish oocytes via intracellular pH-increase and cyclin B-Cdk1 activation

Enako Hosoda[1], Daisaku Hiraoka[2], Noritaka Hirohashi[1,3], Saki Omi[1], Takeo Kishimoto[2], and Kazuyoshi Chiba[1*]

[1]Department of Biological Sciences, Ochanomizu University, Tokyo 112-8610, Japan.

[2]Science & Education Center, Ochanomizu University, Tokyo 112-8610, Japan.

[3] Present address; Oki Marine Biological Station, Education and Research Center for Biological Resources, Shimane 685-0024, Japan

[*]Correspondence to:

Kazuyoshi Chiba: E-mail: chiba.kazuyoshi@ocha.ac.jp, Tel: +81-3-5978-5370

Abstract

Tight regulation of intracellular pH (pH_i) is essential for biological processes. Fully-grown oocytes, having a large nucleus called the germinal vesicle, arrest at meiotic prophase-I. Upon hormonal stimulus, oocytes resume meiosis to acquire fertilizability. At this time, pH_i increases through Na^+/H^+ exchanger activity. However, regulation and function of this change remains obscure. Here we show that in starfish oocytes, serum- and glucocorticoid-regulated kinase (SGK) is activated by the PI3K/TORC2/PDK1 signaling after hormonal stimulus, and is required for the pH_i increase and cyclin B-Cdk1 activation. Furthermore, when we clamped pH_i at 6.7, corresponding to the pH_i of unstimulated ovarian oocytes, hormonal stimulus normally induced cyclin B-Cdk1 activation; thereafter, oocytes initiated germinal vesicle breakdown (GVBD), but failed to complete it. Thus, SGK-dependent pH_i increase is likely prerequisite for completion of GVBD in ovarian oocytes. We propose a model that SGK drives meiotic resumption through concomitant regulation of pH_i and the cell-cycle machinery.

31 **Introduction**

32 Intracellular pH (pH_i) is tightly regulated in living cells. Increases in pH_i are required for a variety of
33 physiological and pathological processes, including early embryonic development[1,2,3] and cancer cell
34 survival[4]. A key pH_i regulator, the sodium–proton exchanger (NHE) is a 12-transmembrane protein
35 that increases pH_i by exporting intracellular H^+ and importing extracellular Na^+ (ref. [5]). Many kinases,
36 including serum- and glucocorticoid-regulated kinase (SGK)[6-8], p90RSK[9], and p38MAPK[10,11],
37 activate NHE in mammalian cells.

38 An NHE-dependent pH_i increase has also been reported during oocyte maturation[12-17], a
39 fundamental process involved in the generation of fertilizable eggs, although the underlying
40 regulatory mechanism and function of pH_i increase during oocyte maturation are not completely
41 understood. In the ovaries of most animals, fully-grown oocytes, which have a large nucleus called
42 the germinal vesicle (GV), are arrested at prophase of meiosis I (ProI)[18]. Upon extracellular stimuli
43 by maturation-inducing hormones, ovarian oocytes resume the meiotic cell cycle via activation of
44 cyclin B–Cdk1 and subsequently undergo germinal vesicle breakdown (GVBD)[19-21]. Subsequently,
45 oocytes undergo another arrest at the metaphase of meiosis I or II (MI or MII arrest) that enables
46 successful fertilization[22]. Starfish oocytes have been used as a model to study oocyte maturation for
47 more than half a century[23]. Previously, we reported that pH_i of ProI-arrested ovarian oocytes is low
48 (~6.7) due to the relatively high CO_2 and low O_2 concentrations in the body cavity of female
49 starfish[17]. Soon after stimulation by the hormone 1-methyladenine (1-MA)[24], pH_i increases to ~6.9[17],
50 after which the oocytes undergo GVBD and ultimately arrest at MI[16,17]. To maintain the MI arrest,
51 pH_i is maintained at ~6.9 until spawning[16,17,25-28]. The increase in pH_i following 1-MA stimulus is
52 known to require starfish NHE3 (sfNHE3)[16,17,25]. However, the upstream signaling and function of
53 this pH_i increase remain elusive.

54 For analysis of pH_i regulation, unstimulated starfish oocytes are isolated from ovaries,
55 placed in artificial seawater (ASW), and used for experiments because various techniques, such as

56 microinjection, are easily applicable to the isolated oocytes. ASW contains relatively low CO_2 and
57 high O_2 relative to the inner body cavity[17]. Due to this difference in gas concentrations, the basal pH_i
58 of isolated oocytes is ~7.0, ~0.3 units higher than that in ovarian oocytes[17]. Soon after 1-MA
59 treatment, this value increases further, to ~7.3, in a sfNHE3-dependent manner[16,17,25]. 1-MA induces
60 Gβγ-dependent activation of phosphoinositide 3-kinase (PI3K)[29-33]. Previously, we demonstrated that
61 the pHi increase is mediated by Gβγ and PI3K[16], although the molecular link between PI3K and the
62 sfNHE3-dependent pH_i increase remains unclear.

63 One candidate for this link is SGK, which is activated downstream of PI3K and
64 upregulates NHE3 in mammalian cells[6,34-36]. Mammalian SGK, which belongs to the AGC kinase
65 family[37], has three isoforms: SGK1, 2, and 3[35,38,39]. All three proteins have an activation-loop
66 (A-loop) and a C-terminal hydrophobic motif (HM)[35], but only SGK3 has the phospholipid-binding
67 domain called the Phox homology domain (PX domain)[39]. Upon agonist stimulation, the HM is first
68 phosphorylated by mammalian target of rapamycin complex 2 (mTORC2) in a PI3K-dependent
69 manner[38-40]. Phosphoinositide-dependent kinase 1 (PDK1) interacts with the phosphorylated HM and
70 phosphorylates the A-loop[41], resulting in full activation of SGK[35,36,42,43]. Although it is not known
71 whether SGK is activated in starfish oocytes, we previously showed that the C-terminus of sfNHE3
72 has a putative consensus sequence for phosphorylation by SGK, and can be phosphorylated by
73 recombinant human SGK1 *in vitro*[25]. Furthermore, PDK1 and TORC2 are functional in starfish
74 oocytes, in which they activate another AGC family kinase, Akt[37], through phosphorylation of its
75 A-loop and the HM[44,45]. In this context, Akt participates in inhibition of Myt1 and activation of
76 Cdc25[32,45-47], leading to cyclin B–Cdk1 activation through dephosphorylation of Cdk1 at Thr14 and
77 Tyr15[23,47]. Collectively, these observations inspired us to investigate whether SGK serves as a
78 downstream mediator of PI3K for the pH_i increase in starfish oocytes.

79 Another issue that remains to be resolved is the role of the pH_i increase following 1-MA
80 stimulation. Previously, we established a method for clamping pH_i at a desired value in starfish

81 oocytes[17], enabling us to examine the effects of altered pH_i. In this study, to elucidate the regulation
82 and function of the pH_i increase in oocytes, we examined the involvement of SGK in the pH_i
83 increase following 1-MA stimulus and the effects of pH_i alteration on meiotic resumption. We found
84 that SGK activation is prerequisite for two mutually independent events: pH_i increase and cyclin
85 B-Cdk1 activation. Moreover, by clamping pH_i at various values, we showed that oocytes exhibit
86 defective GVBD at reduced pH_i values. Based on these findings, we propose a model for
87 SGK-dependent meiotic resumption in starfish ovarian oocytes.

88 **Results**

89 **Starfish SGK is a homolog of human SGK3**

90 To investigate the possible involvement of SGK in the pH_i increase of oocytes during hormonal
91 stimulation with 1-MA in the starfish *A. pectinifera*, we cloned the cDNA of starfish SGK (sfSGK).
92 The open reading frame (ORF) of the cDNA encodes a polypeptide of 489 amino acids with a
93 predicted molecular mass of 56 kDa. At the amino acid sequence level, sfSGK is 52% identical to the
94 human SGK3 PX domain (Fig. 1a, blue open box) and 77% identical to the human SGK3 catalytic
95 domain (Fig. 1a, orange open box). Two phosphorylation sites, which are required for activation of
96 mammalian SGK, are conserved in sfSGK: Thr312 in the A-loop (corresponding to human SGK3
97 Thr320 which is phosphorylated by PDK1), and Thr479 in the HM (human SGK3 Ser486 which is
98 phosphorylated by mTORC2) (Fig. 1a). The transcriptome database contains no other SGK isoforms
99 for *A. pectinifera*, suggesting that SGK3 is the only member of this protein family in starfish.

100 For this study, we generated two types of antibodies: one against a recombinant fragment
101 of sfSGK lacking the N-terminal 50 amino acids (anti-sfSGK-ΔN50), and the other against a
102 C-terminal peptide (17 amino acids) containing the HM of sfSGK (anti-sfSGK-HM). We evaluated
103 the reactivity of these antibodies by immunoblotting starfish oocytes. Both antibodies detected a
104 protein of 56 kDa, corresponding the predicted molecular mass of sfSGK in unstimulated oocytes
105 (Fig. 1b, *left* and *middle* panels), suggesting that these antibodies recognized a sfSGK protein. The
106 sfSGK band underwent a mobility shift after 1-MA treatment (Fig. 1b, *left* and *middle* panels),
107 suggesting that the protein is phosphorylated after 1-MA stimulation.

108 Full activation of mammalian SGK is achieved by PDK1-dependent phosphorylation of
109 A-loop[35,41]. The amino acid sequence of the A-loop in mammalian SGK is quite similar to that of
110 sfSGK (Fig. 1a). Hence, to determine whether sfSGK is phosphorylated in the A-loop in stimulated
111 starfish oocytes, we used a commercial polyclonal anti-human phospho-SGK antibody that
112 recognizes a phosphorylated amino acid in the A-loop of mammalian SGK. The antibody detected a

113 ~59 kDa protein in stimulated oocytes, but not in unstimulated oocytes (Fig. 1b, *right* panel). In
114 addition, this band ran at the same position as the shifted bands recognized by the anti-sfSGK-ΔN50
115 and anti-sfSGK-HM antibodies (Fig. 1b). To confirm that the protein detected by the anti-human
116 phospho-SGK antibody was sfSGK, we immunoprecipitated sfSGK using the anti-sfSGK-HM
117 antibody and immunoblotted with the anti-human phospho-SGK antibody. As expected, we detected
118 protein in the bead fraction (Fig.1 c, *upper* panel, lane 8) but not the flow-through fraction (Fig.1 c,
119 *upper* panel, lane 5), indicating that the anti-human phospho-SGK antibody reacted with sfSGK.
120 Accordingly, hereafter we refer to the A-loop phosphorylation of sfSGK detected by this antibody as
121 "sfSGK-pT312 (A-loop)" in figures. Taken together, these results suggest that sfSGK is
122 phosphorylated at its A-loop, and thereby activated, in oocytes stimulated with 1-MA.
123
124 **sfSGK is activated soon after 1-MA stimulus**
125 To compare the phosphorylation dynamics of sfSGK with Akt, Cdc25 and Cdk1, we treated isolated
126 oocytes with 1-MA and analyzed them by immunoblotting. Mobility shift (Fig. 2a, sfSGK) and
127 A-loop phosphorylation (Fig. 2a, sfSGK-pT312 [A-loop]) of sfSGK was detected 1 min after 1-MA
128 stimulus. The timing of phosphorylation of Akt at Ser477 in HM by TORC2 (ref. [45]) was similar to
129 that of sfSGK (Fig. 2a, Akt-pS477 [HM]). The phosphorylation level of sfSGK increased rapidly,
130 with a peak at 3 min after 1-MA treatment (Fig. 2a, sfSGK-pT312 [A-loop]), followed by a gradual
131 decrease. A band shift of Cdc25 corresponding to hyperphosphorylation[32,47] was detected after 7 min
132 (Fig. 2a, Cdc25). Subsequently, activation of Cdk1 was detectable as dephosphorylation of Tyr15 (ref.
133 [47]) at 10 min (Fig. 2a, Cdk1-pY15), followed by onset of GVBD at approximately 17 min. These
134 results indicate that sfSGK was rapidly activated at the same time as Akt, earlier than Cdc25
135 hyperphosphorylation and cyclin B–Cdk1 activation.
136 Next, we investigated the dynamics of phosphorylation of these proteins in ovarian
137 oocytes in the body cavity, where MI arrest occurs after GVBD[16,17,27]. To this end, we injected 1-MA

138 into the body cavities of female starfish, and then at each time point, isolated two pieces of ovary:
139 one for counting GVBD, and the other for immunoblotting analysis. We found that 95% of ovarian
140 oocytes underwent GVBD within 25 min after 1-MA injection; spawning from the female started at
141 30 min. To prepare ovarian oocytes for immunoblotting, the piece of ovary was placed directly into
142 sample buffer immediately after isolation. Although these samples contained not only oocytes but
143 also other somatic cells derived from ovarian germinal epithelium, we ignored the involvement of
144 the germinal epithelium because the sfSGK, Cdc25 and Cdk1 proteins were not detectable in the
145 germinal epithelium (Fig, 2b). Analysis of oocyte-derived sfSGK, Cdc25, and Cdk1 proteins
146 revealed that both sfSGK and Cdc25 in ovarian oocytes were phosphorylated within 5 min, and that
147 Tyr15 of Cdk1 was dephosphorylated within 25 min (Fig. 2c). These results indicate that sfSGK,
148 Cdc25, and cyclin B–Cdk1 in ovarian oocytes in the body cavity were activated similarly to those in
149 isolated oocytes.
150 It should be noted that the shifted bands of sfSGK (Fig. 2a, sfSGK, lane 11-13; Fig. 2c,
151 sfSGK, lane 4) were maintained even after disappearance of the sfSGK bands reflecting
152 phosphorylation at the A-loop (Fig. 2a, sfSGK-pT312 [A-loop], lanes 11–13; Fig. 2c, sfSGK-pT312
153 [A-loop], lane 4), suggesting the existence of a phosphorylation site outside the A-loop. Given that
154 the phosphorylation site in the HM by TORC2 is conserved in sfSGK, the mobility shift may be due
155 to phosphorylation of the HM.
156
157 **PDK1 and TORC2 phosphorylate sfSGK in a PI3K-dependent manner**
158 Next, we investigated the possible involvement of PDK1 and TORC2 in the activation of sfSGK in
159 starfish oocytes. When we treated oocytes with BX795, a specific inhibitor of PDK1, A-loop
160 phosphorylation of sfSGK after 1-MA treatment was completely blocked (Fig. 2d, lane 10),
161 suggesting that PDK1 is required for A-loop phosphorylation. In mammalian cells, PDK1-dependent
162 phosphorylation of the A-loop requires prior phosphorylation of the HM by mTORC2[36,38,39,41-43]. If

163 this regulation is conserved in starfish, both the A-loop phosphorylation and HM phosphorylation of
164 sfSGK should depend on TORC2. As expected, A-loop phosphorylation was blocked by pp242, a
165 specific inhibitor of TOR, the catalytic subunit of TORC2 (Fig. 2d, lane 6). Notably, the mobility
166 shift of sfSGK was reduced by pp242, but was not affected by BX795 (Fig. 2d, lanes 6 and 10),
167 suggesting that the shift is caused by HM phosphorylation, which is dependent on TORC2 but not
168 PDK1.

169 It should be noted, however, that TOR forms two types of complex: TOR complex 1
170 (TORC1) and TORC2[48], both of which are inhibited by pp242. To confirm that the inhibition of
171 sfSGK phosphorylation by pp242 was due to inhibition of TORC2 rather than TORC1, we used the
172 TORC1 inhibitor rapamycin at a concentration previously shown to be sufficient for inhibition of
173 TORC1 in starfish oocytes[45]. Because neither A-loop phosphorylation nor the mobility shift of
174 sfSGK by 1-MA stimulation was blocked under this condition (Fig. 2d, lane 8), we concluded that
175 TORC2, but not TORC1, phosphorylates sfSGK. Taken together, these observations suggest that
176 sfSGK in starfish oocytes is activated via phosphorylation of the A-loop by PDK1 and of the HM by
177 TORC2, and that the latter is prerequisite for the former. In mammalian cells, PDK1 and TORC2
178 phosphorylate SGK3 downstream of PI3K[35,36,39,43]. Consistent with this, the pan-PI3K inhibitor
179 wortmannin blocked both A-loop phosphorylation and the mobility shift of sfSGK in starfish oocytes
180 (Fig. 2d, lane 4), suggesting that this cascade is conserved in the 1-MA-signaling pathway.

181 To separate fully-activated sfSGK from sfSGK phosphorylated only on the HM, we
182 performed Phos-tag SDS-PAGE, in which phosphorylated proteins migrate more slowly than in
183 normal SDS-PAGE[49]. sfSGK migrated as a single band in unstimulated oocytes (Fig. 2e, the *bottom*
184 band, lane 1). Two additional slower-migrating bands were detected after 1-MA stimulation (Fig. 2e,
185 the *top* and *middle* bands, lane 2). Phosphorylation of the A-loop was detected only in the top band
186 (Fig. 2e, the *top* band, lane 3), suggesting that this band corresponded to fully-activated sfSGK
187 phosphorylated by both PDK1 and TORC2. Indeed, the top band was eliminated by the PDK1

188 inhibitor BX795 and the TORC1/2 inhibitor pp242 (Fig. 2f, the *top* band, lane 5 and 6), but was
189 unchanged by the TORC1 inhibitor rapamycin. In addition, we found that the intensity of the middle
190 band was reduced by pp242, but not by BX795 or rapamycin (Fig. 2f, *middle* band, lanes 5–7),
191 suggesting that it represented sfSGK phosphorylated only on the HM by TORC2. Wortmannin
192 abolished both the top and middle bands (Fig. 2f, lane 4) indicating that all phosphorylation detected
193 using Phos-tag occurred downstream of PI3K. Taken together, these observations suggest that after
194 1-MA stimulus, PDK1 phosphorylates the A-loop of a subset of sfSGK that is pre-phosphorylated on
195 the HM by TORC2 in a PI3K-dependent manner.
196
197 **Activation of sfSGK is required for rapid pH_i increase after 1-MA stimulus**
198 Next, we investigated whether sfSGK is involved in the pH_i increase after 1-MA stimulus. Given that
199 the anti-sfSGK-HM antibody immunoprecipitated sfSGK protein (Fig. 1c), the binding of the
200 antibody to the HM may be strong enough to prevent the interaction of TORC2 with the HM of
201 sfSGK and thereby block phosphorylation of the HM. Indeed, the mobility shift of sfSGK after
202 1-MA stimulus was blocked in oocytes injected with the antibody (Fig. 3a). More importantly,
203 phosphorylation of the A-loop was also blocked (Fig. 3a), as observed in oocytes treated with pp242
204 (Fig. 2d), indicating that the anti-sfSGK-HM antibody inhibited sfSGK activation. This inhibition
205 was specific to sfSGK, because the HM of Akt was phosphorylated even in oocytes pre-injected with
206 the anti-sfSGK-HM antibody (Fig. 3a); accordingly, hereafter we refer to this antibody as an
207 sfSGK-neutralizing antibody. To determine whether sfSGK activation is required for the pH_i increase
208 after 1-MA treatment, we injected a pH-sensitive fluorescent dye, BCECF-dextran, into unstimulated
209 oocytes along with the sfSGK-neutralizing antibody, and monitored the dynamics of pH_i by
210 measuring fluorescence every 30 seconds before and after 1-MA addition. The sfSGK-neutralizing
211 antibody blocked the pH_i increase, whereas the pH_i of oocytes injected with control IgG increased
212 soon after 1-MA treatment (Fig. 3b). These results indicate that the pH_i increase after 1-MA

213 treatment depends on activation of sfSGK.

214

215 **Activation of sfSGK, but not pH_i increase, is required for cyclin B-Cdk1 activation**

216 Previously, we showed that GVBD is initiated by 1-MA in isolated oocytes even when the pH_i

217 increase is blocked[16]. Nonetheless, to our surprise, GVBD was blocked by injection of the

218 sfSGK-neutralizing antibody, whereas control IgG had no inhibitory effects on GVBD (Fig. 4a, b).

219 When we checked the phosphorylation status of Cdc25 and Cdk1 of the oocytes injected with the

220 sfSGK-neutralizing antibody, we found that neither hyperphosphorylation of Cdc25 nor

221 dephosphorylation of Tyr15 of Cdk1 after 1-MA stimulus occurred (Fig, 4c), indicating that this

222 antibody blocked 1-MA–dependent signal transduction leading to cyclin B–Cdk1 activation.

223 To verify that the inhibitory effects of the antibody were caused by specific inhibition of

224 sfSGK activation, we next performed a rescue experiment. Specifically, we replaced Thr479 of

225 sfSGK with Glu (T479E), which was expected to mimic the negatively charged phosphate group,

226 thereby causing PDK1-dependent A-loop phosphorylation even in the presence of the neutralizing

227 antibody. We co-injected mRNA encoding the mutant sfSGK-T479E and the sfSGK-neutralizing

228 antibody into unstimulated oocytes. After a 17-h incubation, the mutant was expressed and partially

229 phosphorylated on its A-loop even in the absence of 1-MA (Fig. 4d). This partial activation did not

230 induce GVBD. 1-MA stimulation induced enhancement of A-loop phosphorylation on the mutant

231 sfSGK (Fig. 4d), as well as GVBD (Fig. 4e), whereas the A-loop phosphorylation and mobility shift

232 of endogenous sfSGK were blocked in these oocytes (Fig. 4d). On the basis of these findings, we

233 concluded that the antibody-injected oocytes are rescued by the additional expression of the mutant

234 sfSGK-T479E, and that the inhibitory effect of the antibody is highly specific.

235 Interestingly, oocytes expressing the T479E mutant underwent GVBD several minutes

236 faster than the control intact oocytes (Fig. 4e), suggesting that partial activation of the mutant in

237 unstimulated oocytes likely shortened the time to GVBD following 1-MA treatment, further

238 supporting the idea that sfSGK participates in 1-MA signaling leading to GVBD. We also found that
239 the band of the T479E mutant phosphorylated on the A-loop underwent an upward mobility shift
240 after 1-MA stimulation, indicating that the mutant was phosphorylated on a site outside the A-loop
241 and the HM; however, the function of this phosphorylation event remains unclear. Taken together,
242 these results suggest that activation of sfSGK is required for cyclin B–Cdk1 activation.
243 Although the 1-MA–induced pH_i increase and cyclin B–Cdk1 activation were
244 simultaneously blocked by the sfSGK-neutralizing antibody, they were independent of each other.
245 We base this claim on two lines of evidence: 1) The increase in pH_i occurred earlier than cyclin B–
246 Cdk1 activation (Fig. 2a, 3b), and was not affected by treatment with the Cdk1 inhibitor, roscovitine
247 (Supplementary Fig. 1), indicating that the pH_i increase is independent of cyclin B–Cdk1 activation.
248 2) GVBD in isolated oocytes, in which initial pH_i before 1-MA stimulation is ~7.0, is initiated even
249 when the pH_i increase was blocked by an NHE inhibitor or by treatment with sodium-free ASW[16],
250 indicating that the cyclin B–Cdk1 activation leading to GVBD is independent of the pH_i increase
251 (see also below, Fig. 5a). Thus, the pH_i increase and cyclin B–Cdk1 activation are mutually
252 independent events.
253
254 **Reduced pH_i delays onset of GVBD and blocks completion of GVBD without affecting cyclin**
255 **B–Cdk1 activation**
256 To elucidate the role of the pH_i increase, we investigated effect of altered pH_i on 1-MA–induced
257 meiotic resumption in starfish oocytes. To clamp pH_i, oocytes were incubated in sodium-free ASW
258 containing CH_3COONH_4 (modified ASW), in which the pH_i was adjusted to the desired value with
259 CH_3COONH_4 but did not increase after 1-MA stimulation because of the absence of sodium ion[17]
260 (see also Materials & Methods). We clamped pH_i at 6.7, corresponding to the value in unstimulated
261 ovarian oocytes[17]; as well as 7.0 and 7.2, similar to the values in isolated oocytes before and after
262 1-MA stimulus, respectively[17]. First, we examined effects of pH_i clamping on sfSGK and cyclin B–

263 Cdk1 activation after 1-MA stimulus. Immunoblotting analysis showed that the phosphorylation
264 status of sfSGK, Cdc25, and Cdk1 in oocytes at all clamped pH_i values was basically same as in
265 oocytes in ASW (Fig. 5a). This observation suggests that 1-MA–induced signaling leading to cyclin
266 B–Cdk1 activation does not depend on pH_i, and further supports our conclusion that the pH_i increase
267 is not required for cyclin B–Cdk1 activation.

268 After cyclin B–Cdk1 activation, the onset of GVBD was delayed for several minutes at a
269 clamped pHi of 6.7 (Fig. 5b), as previously reported[17]. At clamped pH_i values of 7.0 and 7.2, the
270 times of GVBD onset were similar to those in ASW (Fig. 5b). At all clamped pH_i values, the
271 morphology of GVBD onset was indistinguishable from those in ASW: before 1-MA stimulation, the
272 rim of GV looked like a clear line under the microscope; at GVBD onset, cytoplasmic granules
273 started to invade from the rim into the inner GV area (Supplementary Fig. 2). These results suggest
274 that after cyclin B–Cdk1 activation, time to onset of GVBD is weakly pH_i-dependent.

275 More importantly, we observed a remarkable defect after onset of GVBD. In ASW,
276 cytoplasmic granules occupied the whole inner GV area within 15 min after GVBD onset, indicating
277 completion of GVBD (Fig. 5c, Supplementary Movie 1, Supplementary Fig. 3). At a clamped pH_i of
278 6.7, however, we found that the invasion of granules proceeded slowly and stalled around 40 min,
279 remaining incomplete even 60 min after GVBD onset (Fig. 5c, Supplementary Movie 2,
280 Supplementary Fig. 3). At a clamped pH_i of 7.0, invasion proceeded further and finished with a trace
281 of inner GV area within 40–50 min (Fig. 5c, Supplementary Movie 3, Supplementary Fig. 3). At
282 clamped pH_i of 7.2, the granules invaded and ultimately distributed homogenously throughout the
283 oocytes within 20–30 min after GVBD onset (Fig. 5c, Supplementary Movie 4, Supplementary Fig.
284 3). These observations suggest that progression of granule invasion is sensitive to pH_i; in particular,
285 completion of GVBD is drastically impaired at a pH_i of 6.7. Given that the pH_i of unstimulated
286 ovarian oocytes is around 6.7 (ref. [17]), the pH_i increase mediated by sfSGK is likely required for
287 completion of GVBD in ovarian oocytes.

288 **Discussion**

289 The results of this study show that sfSGK is activated by TORC2 and PDK1 in a PI3K-dependent
290 manner after 1-MA stimulus in starfish oocytes. We found that sfSGK is required for regulation of
291 two mutually independent pathways leading to pH_i increase and cyclin B–Cdk1 activation.
292 Furthermore, we identified the presence of a pH_i-sensitive process in meiotic resumption: although
293 1-MA signaling leading to cyclin B–Cdk1 activation is pH_i-independent, the subsequent onset time
294 and completion of GVBD are pH_i-dependent.

295 On the basis of previous studies and the present findings, we propose a model for meiotic
296 resumption in ovarian oocytes (Fig. 6). In this model, sfSGK exerts two essential functions: cyclin
297 B–Cdk1 activation, which induces meiotic resumption, and pH_i increase, which promotes completion
298 of GVBD (Fig. 6). In living starfish, ovarian oocytes reside in coelomic fluid in the body cavity.
299 Previously, we reported that the coelomic fluid has relatively high CO_2 and low O_2 concentrations
300 relative to ASW[17]. Under these gas conditions, the pH_i of unstimulated ovarian oocytes is around 6.7,
301 and increases after 1-MA stimulation[17]. As shown in Fig. 2c, sfSGK is activated in ovarian oocytes
302 after 1-MA stimulus in the body cavity. Subsequently, sfSGK likely induces the pH_i increase and
303 cyclin B–Cdk1 activation in ovarian oocytes (Fig. 6), as demonstrated in isolated oocytes (Figs. 3
304 and 4). Thereafter, cyclin B–Cdk1 causes GVBD. However, if pH_i in ovarian oocytes was not
305 increased from 6.7 soon after 1-MA stimulus, GVBD would initiate after a delay and fail to complete,
306 as we observed when pH_i was clamped at 6.7 in isolated oocytes (Fig. 5). Thus, in ovarian oocytes,
307 the sfSGK-dependent pH_i increase would determine the time of GVBD onset after cyclin B–Cdk1
308 activation and be a prerequisite for completion of GVBD (Fig. 6).

309 In the ovaries, starfish oocytes arrest at MI after GVBD [16,17,27]. This arrest is released upon
310 spawning, at which time the oocytes are ready to be fertilized[16,17,27]. Fertilization during the period
311 between release from the MI arrest and the first polar body formation is important for monospermy,
312 because insemination before GVBD or after polar body formation tends to result in polyspermy[27,50].

313 Thus, the sfSGK-dependent pH_i increase soon after 1-MA may ensure that ovarian oocytes proceed
314 to MI arrest before spawning, helping to promote monospermy. In addition, to ensure fertilization
315 before polar body formation, MI arrest must be maintained until spawning[27]. To maintain MI arrest,
316 sfSGK-dependent pH_i increase should not exceed 7.0, because release from MI arrest occurs at
317 pH_i>7.0 (ref. [16,17,26,27]). In this study, A-loop phosphorylation of sfSGK became undetectable around
318 the time of the end of pH_i increase (Fig. 2a, c). Therefore, sfSGK inactivation may be important to
319 stop the pH_i increase for maintaining MI arrest. Interestingly, the A-loop was dephosphorylated even
320 in the presence of phosphorylated HM (Fig. 2a, c), implying the presence of regulatory mechanism
321 of A-loop dephosphorylation that is not associated with dephosphorylation of the HM, such as
322 up-regulation of an A-loop phosphatase. To our knowledge, regulation of SGK inactivation has never
323 been investigated in any animal, and this issue should be examined in a future study.
324 Although mammalian SGKs are involved in cell proliferation[51,52], their function in
325 M-phase remains unclear. Here, we showed that sfSGK is required for cyclin B–Cdk1 activation in
326 starfish oocytes (Fig. 4). In the accompanying paper, Hiraoka et al. demonstrate that sfSGK directly
327 phosphorylates Cdc25 and Myt1 to activate cyclin B–Cdk1, and that sfSGK, rather than Akt, is the
328 major kinase responsible for induction of cyclin B–Cdk1 activation[53]. These are the first reports to
329 demonstrate the involvement of SGK in cyclin B–Cdk1 activation.
330 In addition, we showed that sfSGK is required for the pH_i increase (Fig. 3b). Previously,
331 we reported that this increase depends on sfNHE3[16,17,25]. In human cultured cells, NHE-dependent
332 pH_i increase is upregulated by phosphorylation of C-terminal region of NHE that leads to NHE
333 activation[7,9], and/or by accumulation of NHE protein on the plasma membrane through trafficking of
334 endosomal NHE to the plasma membrane[6]. Although it is not known whether these mechanisms are
335 functional in starfish oocytes, it is clear from our previous work that the C-terminus of sfNHE3 is
336 phosphorylated by human SGK1 *in vitro*[25]. Therefore, we speculate that sfSGK upregulates sfNHE3
337 by direct phosphorylation of its C-terminus.

338 In the process of GVBD in starfish oocytes, the nuclear pore complex on nuclear envelopes
339 (NEs) of the GV are first disassembled[54-56], and then the NEs are rapidly broken into membrane
340 fragments, followed by complete mixing of cytoplasm and nucleoplasm[54,55]. GVBD onset, as judged
341 by differential interference contrast (DIC) microscopy in this study, likely represents the time of
342 membrane fragmentation, as a clear boundary between cytoplasm and GV was still observed by DIC
343 during nuclear pore disassembly[55]. One possible interpretation of the remarkable blockage of GVBD
344 completion at a clamped pH_i of 6.7 (Fig. 5b, c) is that incomplete NE fragmentation occurred and
345 disrupted invasion of cytoplasmic granules. Given that NE fragmentation depends on F-actin shell
346 formed on the inner surface of the GV[56], our present observations imply that the formation or
347 function of this shell is blocked at pH_i 6.7. Although this possibility is yet to be tested, F-actin
348 architecture is known to be disrupted by lower pH_i, at least in mouse mammary tissue[57].
349 pH_i increase after release from ProI arrest has also been reported in frog[13], urodele[58], and
350 surf clam[12]. In *Xenopus* oocytes, NHE-dependent pH_i increase after hormonal stimulation[13,14,59] has
351 been suggested to accelerate cyclin B–Cdk1 activation by promoting accumulation of Mos protein,
352 which participates in cyclin B–Cdk1 activation[60]. By contrast, we found that cyclin B–Cdk1
353 activation was independent of the pH_i increase. One potential reason for this difference could be
354 cyclin B–Cdk1 activation in starfish oocytes does not require synthesis of new protein[61], including
355 Mos[62]. In addition, pH_i increase in *Xenopus* oocytes plays a role in migration of GV to the animal
356 pole before GVBD[63]. Such migration does not occur in starfish oocytes because the GV already
357 resides at the animal pole even in ProI-arrested oocytes. Instead, we found that completion of GVBD
358 depends on pHi. Thus, starfish and *Xenopus* oocytes provide suitable models for understanding
359 different aspects of pH_i-dependent regulation of the meiotic cell cycles.
360 In summary, we showed that sfSGK is required for pH_i increase and cyclin B–Cdk1
361 activation in starfish oocytes, and that completion of GVBD is a pH_i-sensitive process. These
362 findings reveal a novel role for SGK in control of meiotic cell cycles and emphasize the importance

363 of tight regulation of pH_i in oocyte meiosis.

364 **Materials and methods**

365 **Oocyte preparation.** Starfish (*Asterina pectinifera*) were collected on Pacific coast of Japan, and
366 kept in laboratory aquaria supplied with circulating seawater at 14°C. Fully-grown ProI-arrested
367 oocytes were isolated from ovaries and treated with calcium-free artificial seawater (calcium-free
368 ASW: 476 mM NaCl, 10 mM KCl, 36 mM $MgCl_2$, 18 mM $MgSO_4$, 20 mM H_3BO_3, pH 8.2) to
369 remove follicle cells. Subsequently, the oocytes were kept in artificial seawater (ASW: 462 mM
370 NaCl, 10 mM $CaCl_2$, 10 mM KCl, 36 mM $MgCl_2$, 18 mM $MgSO_4$, 20 mM H_3BO_3, pH 8.2) until use.
371 For 1-MA stimulation, the isolated oocytes were incubated with ASW containing 0.5 μM 1-MA at
372 23°C, and then collected for analysis. To induce meiotic resumption of ovarian oocytes in the body
373 cavity, 1 ml of calcium-free ASW without boric acid (462 mM NaCl, 10 mM KCl, 36 mM $MgCl_2$, 17
374 mM $MgSO_4$) containing 0.5 mM 1-MA was injected into the body cavity of female starfish. Pieces of
375 ovary containing stimulated oocytes were directly recovered from the body cavity, and then
376 immediately added into a sample buffer (0.25 M Tris-HCL [pH 6.8], 40% glycerol, 8% SDS, 20%
377 2-mercaptoethanol, 0.01% bromophenol blue). To compare proteins in germinal epithelium with
378 those in oocytes, a piece of ovary was isolated from the body cavity and separated into germinal
379 epithelium and oocytes. These fractions were separately recovered into different tubes, each of which
380 contained an equal volume of sample buffer, boiled at 95°C for 5 min, and subjected to
381 immunoblotting analysis.

382

383 **cDNA cloning of starfish SGK.** To isolate a cDNA encoding the starfish homolog of SGK, total
384 mRNA was isolated from ProI-arrested ovarian oocytes using RNAwiz (Ambion, Thermo Fisher
385 Scientific; Waltham, MA, USA). The first-strand cDNA library was prepared from total mRNA using
386 the TAKARA RNA PCR Kit (AMV) Ver.2.1 and Prime Script Reverse Transcriptase (Takara Bio;
387 Shiga, JP) with random 9-mers. A 250-bp cDNA fragment (fragment 1) was first obtained by
388 reverse-transcriptase (RT)-PCR with degenerate primers designed based on amino acid sequences

389 conserved among human, mouse, sea urchin, and *C. elegans* SGKs (forward: YAVKVL,
390 5'-TAYGCNGTNAARGTNYT-3', and reverse: FYAAEIA, 5'-AARATRCGNCGNCTYTCDCG-3').
391 Because 3' and 5' rapid amplification of cDNA ends (RACE) with specific primers designed against
392 fragment 1 were unsuccessful, we obtained another fragment (fragment 2) that partially overlapped
393 with fragment 1, as follows: a forward specific primer (5'-CCCGACAAGCTCTAC-3') was
394 designed against fragment 1, and a reverse degenerate primer (GLPPFY,
395 5'-CCNRANGGNGGNAARAT-3') was designed against a conserved amino acid sequence in the
396 SGK alignment that is located in a region approximately 85 amino acids C-terminal to the region of
397 the first reverse degenerate primer. The 360-bp fragment 2 was obtained by RT-PCR using these
398 primers. Next, to identify the 3' end, another first-strand cDNA library was generated from the total
399 mRNA using RNA PCR Kit (AMV) Ver. 2.1 and Prime Script Reverse Transcriptase (Both, Takara
400 Bio; Shiga, JP) using the oligo dT-Adaptor primer from the kit. Then, RT-PCR was performed on the
401 cDNA library using a specific forward primer designed against the 5' region of fragment 2
402 (5'-CCCCAGAAGTCTTGAAGAA-3') and the adaptor primer (5'-GTTTTCCCAGTCACGAC-3').
403 Using the RT-PCR product as a template, nested PCR was performed with another forward specific
404 primer (5'-GGAGTATGATCGTAGTGTAG-3') and the adaptor primer, resulting in amplification of
405 a ~600 bp 3' RACE product. Next, the 5' ends were identified by RACE using 5'-Full RACE Core
406 Set (Takara Bio; Shiga, JP) with specific primers (reverse for generating first-strand cDNA:
407 5'-CCAAAGTCTGTCAAC-3'; forward for first PCR: 5'-CAGAGATTTGAAGCCGGAG-3',
408 reverse for first PCR: 5'-GTTCAGGGAAGCATCTCTTCT-3'; forward for nested PCR:
409 5'-GCCGGAGAACATTTTGATTG-3', reverse for nested PCR:
410 5'CTCTCTCTGCAGATGGAAGA-3'), resulting in amplification of a 1.5-kb 5' RACE product. The
411 full-length ORF was PCR-amplified from the cDNA library generated using random 9mers with
412 pfx50 DNA polymerase (Thermo Fisher Scientific) and specific primers (forward:
413 5'-GGGGCCCCTGGGATCCATGGCTGCCAACAGTACTAG-3'; reverse:

414 5'-GTCGACCCGGGAATTCTTAGTCGTCAAATGCCTCG-3'). The amplified cDNA was inserted
415 into vector pGEX-6P-3 (GE Healthcare; Little Chalfont, UK) using the In-Fusion HD Cloning Kit
416 (Takara Bio; Shiga, JP) and sequenced.
417
418 **Immunoprecipitation.** For preparation of oocyte extracts, oocytes were recovered in ASW before
419 and after 1-MA treatment. After freezing in liquid N_2, lysis buffer [80 mM β-glycerophosphate, 20
420 mM EGTA, 10 mM Mops pH 7.0, 100 mM sucrose, 100 mM KCl, 1 mM DTT, 0.5 % NP-40, 1%
421 protease inhibitor cocktail (Nacalai Tesque; Kyoto, JP), and 1% phosphatase inhibitor cocktails 1 and
422 2 (Sigma; St Louis, MO, USA)] was added to the oocytes, followed by vortexing and centrifugation
423 at 12,500× *g* for 15 min. The supernatant was used as the extract. For immunoprecipitation, 15 μl of
424 oocyte extract (1 oocyte per 1 μl) was added to 3 μl of protein A–Sepharose 4B (Sigma) to which 7.0
425 μg of anti-sfSGK-HM antibody or control IgG had been pre-adsorbed and cross-linked using borate
426 buffer containing 25 mM DSS (25 mM DSS, 0.2 M H_3BO_3 [pH 9.0], 0.2 M NaOH), followed by
427 incubation for 90 min on ice. Beads and flow-through were separated, and sample buffer was added.
428 The samples were boiled at 95°C for 5 min and subjected to immunoblotting analysis.
429
430 **Chemicals.** Wortmannin (LC laboratories; Woburn, MA, USA), pp242 (Cayman Chemical; Ann
431 Arbor, MI, USA), rapamycin (FUJIFILM Wako pure chemical; Osaka, JP), BX795 (Enzo Life
432 Sciences; New York, NY, USA), and roscovitine (Merck, Darmstadt, BRD) were dissolved in DMSO
433 at 20 mM as a stock solution, and used at final concentrations of 40, 2, 20, 6, and 30 μM,
434 respectively.
435
436 **DNA construct.** A mutant sfSGK in which Thr479 was replaced with Glu was generated by PCR
437 using PrimeSTAR MAX Polymerase (Takara Bio; Shiga, JP) with primers containing the point

438 mutation (forward: 5'-GGCTTCGAATATGTCCCACCAAGCGAG-3', and reverse:
439 5'-GACATATTCGAAGCCAGTAAAGGCAGAG-3'). The mutated cDNA was inserted into the
440 pSP64-S-based vector, in which its SP6 promoter was replaced with a T7 promoter[32], with the *A.*
441 *pectinifera* cyclin B Kozak sequence (5'-TACAAT-3') and a 3× FLAG-tag at C-terminus.
442
443 **Antibodies.** The anti-sfSGK-ΔN50 rabbit polyclonal antibody was raised against a Nus- and
444 His-tagged recombinant sfSGK fragment lacking the N-terminal 50 amino acids including the PX
445 domain. The antibody was purified from the antiserum using PVDF membrane on which a
446 recombinant GST-tagged sfSGK protein had been blotted. The anti-sfSGK-HM rabbit polyclonal
447 antibody was raised against a synthetic peptide representing the 17 C-terminal amino acids
448 containing the HM (Ser473-Asp489) of sfSGK, and affinity-purified using antigen peptide–
449 conjugated Sulfo Link Coupling Resin (Thermo Fisher Scientific). The control IgG was purified
450 from rabbit pre-immune serum using protein A–Sepharose 4B (Sigma). For microinjection, the
451 anti-sfSGK-HM antibody and control IgG were further concentrated using a 50-kDa cut-off Amicon
452 Ultra (Merck; Rahway, NJ, USA), and the buffer was replaced with injection buffer (0.05% NP-40 in
453 PBS buffer, pH 7.2). Preparation of anti-starfish phospho-Akt (Ser477) rabbit polyclonal antibody[45],
454 anti-starfish Akt (sfAkt) C-terminus rabbit polyclonal antibody[46], anti-starfish Cdc25 (sfCdc25)
455 rabbit polyclonal antibody[47], and anti-PSTAIR antibody for Cdk1 (ref. [45]) were described previously.
456 The anti-phospho-Tyr15 Cdk1 antibody and anti-human phospho-SGK rabbit polyclonal antibody
457 [p-SGK (Thr 256)-R] were purchased from Cell Signaling Technology (Danvers, MA, USA) and
458 Santa Cruz Biotechnology (Dallas, TX, USA), respectively. Peroxidase-conjugated anti-rabbit IgG
459 and anti-mouse IgG, used as secondary antibodies in immunoblotting, were purchased from GE
460 healthcare (Little Chalfont, UK) and Dako (Glostrup, Denmark), respectively.
461

462 **Microinjection.** Microinjection was performed as previously described[64,65]. The anti-sfSGK-HM
463 antibody or control IgG was injected into unstimulated oocytes at 23°C at a final concentration in the
464 oocyte of 65.2 μg/ml, followed by incubation for 1 h. For expression of sfSGK (T479E), the mutant
465 was transcribed from the pSP64-S-based vector construct using the mMESSAGE mMACHINE kit
466 (Ambion, Thermo Fisher Scientific), dissolved in water, and injected into unstimulated oocytes (30
467 pg per oocyte). After further incubation for 17 h at 20°C, these oocytes were treated with 0.5 μM
468 1-MA and recovered for immunoblotting analysis at 4 min. The rest of the oocytes were observed to
469 count GVBD.
470
471 **Immunoblotting.** Oocytes (five for normal SDS-PAGE, six for Phos-tag-SDS-PAGE) were
472 recovered in 3 μl of seawater, added directly to 3 μl of 2× sample buffer, and immediately frozen in
473 liquid N_2. After thawing and boiling for 5 min at 95°C, proteins were separated on polyacrylamide
474 gels (8% for sfSGK only, 8.5% for sfSGK and Cdk1). For Phos-tag SDS-PAGE, 8% polyacrylamide
475 gel containing 60 μM Phos-tag acrylamide (FUJIFILM Wako Pure Chemical co.; Osaka, JP) and 600
476 μM $ZnCl_2$ was used. Immunoblotting was performed as previously described[32]. Antibodies used for
477 immunoblotting were as follows: anti-sfSGK-ΔN50 (1:2,000, in TBS-T), anti-sfSGK-HM (1:1000,
478 in TBS-T), anti-human phospho-SGK (1:400, in TBS-T), anti-sfAkt-pS477 (1:600, in Can Get Signal
479 Immunoreaction Enhancer Solution 1 [Can Get sol. 1], TOYOBO, Osaka, Japan),
480 anti-sfAkt-C-terminus (1:400, in Can Get sol. 1), anti-sfCdc25 (1:2000, in Can Get sol. 1), an
481 anti-Cdk1-pY15 (1:1000, in Can Get sol. 1), and anti-PSTAIR (1:50,000, in Can Get sol. 1).
482 horseradish peroxidase (HRP)-conjugated anti-rabbit IgG (1: 2000, in TBS-T or Can Get sol. 2) and
483 anti-mouse IgG (1:2000, in Can Get sol. 2) were used as secondary antibodies. Proteins reacting with
484 the antibodies were visualized with ECL prime (GE healthcare; Little Chalfont, UK), and digital
485 images were acquired on a LAS4000 mini imager (Fujifilm; Tokyo, JP).
486

487 **Measurement of pH_i with BCECF-dextran.** A dextran (10-kDa)-conjugate of
488 2',7'-bis-(2-carboxyethyl)-5(and-6)-carboxyfluorescein (BCECF) (Molecular Probes, Thermo Fisher
489 Scientific) was dissolved at a concentration of 2 mM in injection buffer (100 mM potassium
490 aspartate, 10 mM HEPES, 0.05% NP-40, pH 7.2). BCECF-dextran (20 pl per oocyte) and either the
491 sfSGK-HM antibody or control IgG (final 65.2 μg /ml in an oocyte) were co-injected into
492 unstimulated oocytes. After incubation for 1 h, the pH_i of these oocytes was measured every 30
493 seconds before and after 1-MA treatment. pH_i measurements with BCECF-dextran were made by
494 determining the pH-dependent ratio of its emission intensity (detected at 535 nm) when excited at
495 495 nm versus its isosbestic point of 436 nm. Calibration of pH_i from the intensity ratio was
496 performed as previously described[17]. All fluorescence images were captured and analyzed using a
497 NIKON ECLIPSE Ti-U fluorescent microscope (Nikon Instech; Tokyo, JP), which was connected to
498 a CMOS camera (ORCA-Flash2.8, C11440-10C; Hamamatsu Photonics; Hamamatsu, JP) controlled
499 by an HCImage processing system (Hamamatsu Photonics; Hamamatsu, JP). Excitation light from a
500 xenon lamp alternated between 436 nm and 495 nm under computational control. The emitted light
501 passed through a dichroic beam splitter at 505 nm and through a 510–560 nm emission filter.
502
503 **Clamping pH_i of oocytes.** NH_4Cl dissolved in seawater forms NH_3, which crosses cell membrane
504 easily and binds H^+, causing an increase in pH_i. By contrast, when CH_3COONa is dissolved in
505 seawater, it forms CH_3COOH, which crosses cell membrane easily and releases H^+ into the cell,
506 causing pHi to decrease. By applying this principle, Hamaguchi *et al.* found that extracellular pH
507 (pH_o) and pH_i were almost equal when sea urchin eggs were treated with ASW containing 20 mM
508 CH_3COONa and NH_4Cl[66]. We showed previously that when starfish oocytes are incubated in
509 sodium-free ASW containing CH_3COONH_4 at various pH values (modified ASW: 480 mM choline
510 chloride, 55 mM $MgCl_2$, 5 mM KCl, 10 mM PIPES, 10 mM HEPES, 20 mM CH_3COONH_4, 9.2 mM
511 $CaCl_2$), the pH_i of oocytes was invariably ~0.2 units higher than pH_o[17]. Hence, to clamp pH_i of

512 oocytes at 6.7, 7.0, and 7.2, unstimulated oocytes were incubated with modified ASW with a pH of
513 6.5, 6.8, and 7.0, respectively, for 20 min. These oocytes were then treated with 1-MA, followed by
514 observation of GVBD or immunoblotting analysis. It should be noted that because sodium ion is not
515 present in modified ASW, the sfNHE3-dependent pH_i increase mediated by Na^+/H^+ exchange does
516 not occur, so pHi is maintained at the clamped value even after 1-MA treatment. As a control,
517 isolated oocytes were incubated in ASW (pH_o 8.2), in which the pHi of unstimulated oocytes was
518 ~7.0. Because ASW contains sodium ions, a sfNHE3-dependent pH_i increase to 7.2–7.3 occurs after
519 1-MA treatment[17]; see also the control IgG–injected oocytes in Fig. 3b.

520 **Oocyte observation.** GVBD onset was visually judged by focusing the microscope on the equatorial
521 plane of the GV: the rim of intact GV appears as a sharp line in unstimulated oocytes, but becomes
522 fuzzy at GVBD onset. All DIC images and DIC image sequences were captured on a NIKON
523 ECLIPSE Ti-U microscope (Nikon Instech; Tokyo, JP), which was connected to a CMOS camera
524 (ORCA-Flash2.8, C11440-10C; Hamamatsu Photonics; Hamamatsu, JP) controlled by a HCImage
525 processing system (Hamamatsu Photonics; Hamamatsu, JP). For time-lapse recording, DIC images
526 were collected every 10 seconds. Z-stack images were captured soon after time-lapse imaging.

527 **Data availability**

528 Data supporting the findings of this study are available within the article or upon reasonable request
529 to the corresponding authors.

530

531 **Acknowledgements**

532 We thank M. Matsushita for raising the anti-starfish SGK-ΔN50 antibody, M. Terasaki for providing
533 vector pSP64-S, and E. Okumura for providing anti-sfCdc25 and anti-sfAkt C-terminus antibodies.
534 We also thank K. Yura for his contribution to perform alignment of SGK isoforms. This work was
535 supported by JSPS KAKENHI grant numbers 17K07405, Takeda Science Foundation, and the
536 Cooperative Program provided by The Atmosphere and Ocean Research Institute, The University of
537 Tokyo.

538

539 **Author contributions**

540 E.H., D.H., and K.C. conceived and designed all the experiments, and E.H. performed all the
541 experiments. Cloning of cDNA encoding sfSGK was performed by S.O. and N.H. All authors
542 discussed the results. E.H., D.H., T.K., and K.C. wrote the manuscript.

543

544 **Competing interests**

545 The authors declare no competing interests.

546

547 **Materials and correspondence**

548 Correspondence and requests for materials should be addressed to K.C.

549 **References**

550 1. Baltz, J. M. Intracellular pH regulation in the early embryo. *Bioessays* **15**, 523–530 (1993).

551 2. Schatten, G., Bestor, T., Balczon, R., Henson, J. & Schatten, H. Intracellular pH shift initiates
552 microtubule-mediated motility during sea urchin fertilization. *Ann. N. Y. Acad. Sci.* **466**, 940–944
553 (1986).

554 3. Grandin, N. & Charbonneau, M. Cycling of intracellular pH during cell division of Xenopus
555 embryos is a cytoplasmic activity depending on protein synthesis and phosphorylation. *J. Cell*
556 *Biol.* **111**, 523–532 (1990).

557 4. Grillo-Hill, B., Choi, C., Jimenez-Vidal, M. & Barber, D. Increased H^+ efflux is sufficient to
558 induce dysplasia and necessary for viability with oncogene expression. *Elife* **4**, 10.7554/eLife.03270.
559 (2015).

560 5. Orlowski, J. & Grinstein, S. Diversity of the mammalian sodium/proton exchanger SLC9 gene
561 family. *Pflugers Archi.* **447**, 549–565 (2004).

562 6. He, P. et al. Serum- and glucocorticoid-induced kinase 3 in recycling endosomes mediates acute
563 activation of Na^+/H^+ exchanger NHE3 by glucocorticoids. *Mol. Biol. Cell* **22**, 3812–3825 (2011).

564 7. Wang, D., Sun, H., Lang, F. & Yun, C. Activation of NHE3 by dexamethasone requires
565 phosphorylation of NHE3 at Ser663 by SGK1. *Am J Physiol. Cell Physiol.* **289**, C802–C810 (2005).

566 8. Yun, C. C. Concerted roles of SGK1 and the Na^+/H^+ exchanger regulatory factor 2 (NHERF2) in
567 regulation of NHE3. *Cell Physiol. Biochem.* **13**, 29–40 (2003).

568 9. Takahashi, E. et al. $p90^{RSK}$ is a serum-stimulated Na^+/H^+ exchanger isoform-1 kinase.
569 Regulatory phosphorylation of serine 703 of Na^+/H^+ exchanger isoform-1. *J. Biol.*
570 *Chem.* **274**, 20206–20214 (1999).

571 10. Wang, C. et al. Somatostatin stimulates intestinal NHE8 expression via p38 MAPK
572 pathway. *Am. J. Physiol. Cell Physiol.* **300**, C375–C382 (2011).

573 11. Xu, H., Ghishan, F. & Kiela, P. SLC9 gene family: function, expression, and regulation. *Copr.*
574 *Physiol.* **8,** 555–583 (2018).
575 12. Dubé, F. & Eckberg, W. Intracellular pH increase driven by an Na^+/H^+ exchanger upon
576 activation of surf clam oocytes. *Dev. Biol.* **190**, 41–54 (1997).
577 13. Lee, S. & Steinhardt, R. pH changes associated with meiotic maturation in oocytes of Xenopus
578 laevis. *Dev. Biol.* **85,** 358–369 (1981).
579 14. Rezai, K., Kulisz, A. & Wasserman, W. J. Protooncogene product, c-mos kinase, is involved in
580 upregulating Na^+/H^+ antiporter in Xenopus oocytes. *Am. J. Physiol.* **267**, C1717–1722 (1994).
581 15. Miyazaki SI, Ohmori H, & Sasaki S. Potassium rectifications of the starfish oocyte membrane
582 and their changes during oocyte maturation. *J. Physiol.* **246**, 55-78. (1975)
583 16. Harada, K., Oita, E. & Chiba, K. Metaphase I arrest of starfish oocytes induced via the MAP
584 kinase pathway is released by an increase of intracellular pH. *Development* **130,** 4581–4586 (2003).
585 17. Moriwaki, K., Nakagawa, T., Nakaya, F., Hirohashi, N. & Chiba, K. Arrest at metaphase of
586 meiosis I in starfish oocytes in the ovary is maintained by high CO_2 and low O_2 concentrations in
587 extracellular fluid. *Zoolog. Sci.* **31**, 975–984 (2013).
588 18. Masui, Y. From oocyte maturation to the *in vitro* cell cycle: the history of discoveries of
589 Maturation-Promoting Factor (MPF) and Cytostatic Factor (CSF). *Differentiation* **69**, 1–17 (2001).
590 19. Hunt, T. Maturation promoting factor, cyclin and the control of M-phase. *Curr. Opin. Cell*
591 *Biol.* **1**, 268–274 (1989).
592 20. Nurse, P. Universal control mechanism regulating onset of M-phase. *Nature* **344**, 503–508
593 (1990).
594 21. Kishimoto, T. Entry into mitosis: a solution to the decades-long enigma of MPF. *Chromosoma*
595 **124**, 417–428 (2015).
596 22. Chiba, K. Evolution of the acquisition of fertilization competence and polyspermy blocks
597 during meiotic maturation. *Mol. Reprod. Dev.* **78**, 808–813 (2011).

598 23. Kishimoto, T. MPF-based meiotic cell cycle control: Half a century of lessons from starfish
599 oocytes. *Proc. Jpn. Acad. Ser. B. Phys. Biol. Sci.* **94**, 180–203 (2018).
600 24. Kanatani, H., Shirai, H., Nakanishi, K. & Kurokawa, T. Isolation and indentification of meiosis
601 inducing substance in starfish *Asterias amurensis*. *Nature* **221**, 273–274 (1969).
602 25. Harada, K., Fukuda, E., Hirohashi, N. & Chiba, K. Regulation of intracellular pH by
603 p90Rsk-dependent activation of an Na^+/H^+ exchanger in starfish oocytes. *J. Biol. Chem.* **285**, 24044–
604 24054 (2010).
605 26. Oita, E., Harada, K. & Chiba, K. Degradation of polyubiquitinated Cyclin B is blocked by the
606 MAPK pathway at the Metaphase I arrest in starfish oocytes. *J. Biol. Chem.* **279**, 18633–18640
607 (2004).
608 27. Usui, K., Hirohashi, N. & Chiba, K. Involvement of mitogen-activating protein kinase and
609 intracellular pH in the duration of the metaphase I (MI) pause of starfish oocytes after spawning. *Dev.*
610 *Growth Differ.* **50**, 357–364 (2008).
611 28. Ochi, H., Aoto, S., Tachibana, K., Hara, M. & Chiba, K. Block of CDK1-dependent
612 polyadenosine elongation of Cyclin B mRNA in metaphase-I-arrested starfish oocytes is released by
613 intracellular pH elevation upon spawning. *Mol. Reprod. Dev.* **83**, 79–87 (2016).
614 29. Shilling, F., Chiba, K., Hoshi, M., Kishimoto, T. & Jaffe, L. Pertussis toxin inhibits
615 1-methyladenine-induced maturation in starfish oocytes. *Dev. Biol.* **133**, 605–608 (1989).
616 30. Chiba, K., Kontani, K., Tadenuma, H., Katada, T. & Hoshi, M. Induction of starfish oocyte
617 maturation by the βγ subunit of starfish G protein and possible existence of the subsequent effector in
618 cytoplasm. *Mol. Biol. Cell* **4**, 1027– 1034 (1993).
619 31. Sadler, K. & Ruderman, J. Components of the signaling pathway linking the 1-methyladenine
620 receptor to MPF activation and maturation in starfish oocytes. *Dev. Biol.* **197**, 25–38 (1998).

621 32. Hiraoka, D., Aono, R., Hanada, S., Okumura, E. & Kishimoto, T. Two new competing
622 pathways establish the threshold for cyclin-B–Cdk1 activation at the meiotic G2/M transition. *J. Cell*
623 *Sci.* **129**, 3153–3166 (2016).
624 33. Vanhaesebroeck, B., Guillermet-Guibert, J., Graupera, M. & Bilanges, B. The emerging
625 mechanisms of isoform-specific PI3K signalling. *Nat. Rev. Mol. Cell Biol.* **11**, 329-341 (2010).
626 34. Tessier, M. & Woodgett, J. Serum and glucocorticoid-regulated protein kinases: Variations on a
627 theme. *J. Cell Biochem.* **98**, 1391–1407 (2006).
628 35. Kobayashi, T., Deak, M., Morrice, N. & Cohen, P. Characterization of the structure and
629 regulation of two novel isoforms of serum- and glucocorticoid-induced protein kinase. *Biochem.*
630 *J.* **344**, 189–197 (1999).
631 36. Malik, N. et al. Mechanism of activation of SGK3 by growth factors via the Class 1 and Class 3
632 PI3Ks. *Biochem. J.* **475,** 117–135 (2018).
633 37. Pearce, L., Komander, D. & Alessi, D. The nuts and bolts of AGC protein kinases. *Nat. Rev.*
634 *Mol. Cell Biol.* **11**, 9–22 (2010).
635 38. Kobayashi, T. & Cohen, P. Activation of serum- and glucocorticoid-regulated protein kinase by
636 agonists that activate phosphatidylinositide 3-kinase is mediated by 3-phosphoinositide-dependent
637 protein kinase-1 (PDK1) and PDK2. *Biochem. J.* **339**, 319–328 (1999).
638 39. Tessier, M. & Woodgett, J. R. Role of the Phox homology domain and phosphorylation in
639 activation of serum and glucocorticoid-regulated kinase-3. *J. Biol. Chem.* **281**, 23978–23989 (2006).
640 40. García-Martínez, J. M. & Alessi, D. R. mTOR complex 2 (mTORC2) controls hydrophobic
641 motif phosphorylation and activation of serum- and glucocorticoid-induced protein kinase 1 (SGK1).
642 *Biochem. J.* **416**, 375–385 (2008).
643 41. Biondi, RM., Kieloch, A., Currie, RA., Deak, M. & Alessi, DR. The PIF-binding pocket in
644 PDK1 is essential for activation of S6K and SGK, but not PKB. *EMBO J.* **20**, 4380-4390 (2001).

645 42. Lu, M. et al. mTOR Complex-2 Activates ENaC by Phosphorylating SGK1. *J. Am. Soc.*
646 *Nephrol.* **21,** 811–818 (2010).
647 43. Lien, E. C., Dibble, C. C. & Toker, A. PI3K signaling in cancer: beyond AKT. *Curr. Opin. Cell*
648 *Biol.* **45**, 62–71 (2017).
649 44. Hiraoka, D. et al. PDK1 is required for the hormonal signaling pathway leading to meiotic
650 resumption in starfish oocytes. *Dev. Biol.* **276**, 330–336 (2004).
651 45. Hiraoka, Okumura & Kishimoto, T. Turn motif phosphorylation negatively regulates activation
652 loop phosphorylation in Akt. *Oncogene* **30**, 4487–4497 (2011).
653 46. Okumura, E. et al. Akt inhibits Myt1 in the signalling pathway that leads to meiotic
654 G2/M-phase transition. *Nat. Cell. Biol.* **4**, 111–116 (2002).
655 47. Okumura, E., Sekiai, T., Hisanaga, S., Tachibana, K. & Kishimoto, T. Initial triggering of
656 M-phase in starfish oocytes: a possible novel component of maturation-promoting factor besides
657 cdc2 kinase. *J. Cell Biol.* **132**, 125–135 (1996).
658 48. Eltschinger, S. & Loewith, R. TOR complexes and the maintenance of cellular
659 homeostasis. *Trends Cell Biol.* **26**, 148–159 (2016).
660 49. Kinoshita, E., Kinoshita-Kikuta, E., Takiyama, K. & Koike, T. Phosphate-binding Tag, a New
661 Tool to Visualize Phosphorylated Proteins. *Mol. Cell Proteomics* **5,**749–757 (2006).
662 50. Miyazaki, S. & Hirai, S. Fast polyspermy block and activation potential correlated changes
663 during oocyte maturation of a starfish. *Dev. Biol.* **70**, 327–340 (1979).
664 51. Hayashi, M. et al. BMK1 mediates growth factor-induced cell proliferation through direct
665 cellular activation of SGK. *J. Biol. Chem.* **276**, 8631–8634 (2001).
666 52. Gasser, J. et al. SGK3 mediates INPP4B-dependent PI3K signaling in breast cancer. *Mol.*
667 *Cell* **56**, 595–607 (2014).
668 53. Hiraoka, D., Hosoda, E., Chiba, K. & Kishimoto, T. SGK phosphorylates Cdc25 and Myt1 to
669 trigger cyclin B-Cdk1 activation at the meiotic G2/M transition. Accompanying manuscript (2018).

670 54. Terasaki, M. et al. A new model for nuclear envelope breakdown. *Mol. Biol. Cell* **12**, 503–510
671 (2001).
672 55. Lénárt, P. et al. Nuclear envelope breakdown in starfish oocytes proceeds by partial NPC
673 disassembly followed by a rapidly spreading fenestration of nuclear membranes. *J. Cell*
674 *Biol.* **160**, 1055–1068 (2003).
675 56. Mori, M. et al. An Arp2/3 nucleated F-actin shell fragments nuclear membranes at nuclear
676 envelope breakdown in starfish oocytes. *Curr. Bio.* **24**, 1421–1428 (2014).
677 57. Jenkins, E., Debnath, S., Varriano, S., Gundry, S. & Fata, J. Na^+/H^+ exchanger 1 (NHE1)
678 function is necessary for maintaining mammary tissue architecture. *Dev. Dyn.* **243**, 229–242 (2014).
679 58. Rodeau, J. L. & Vilain, J. P. Changes in membrane potential, membrane resistance, and
680 intracellular H^+, K^+, Na^+, and Cl^- activities during the progesterone-induced maturation of urodele
681 amphibian oocytes. *Dev. Biol.* **120**, 481–493 (1987).
682 59. Stith, B. & Maller, J. Increased intracellular pH is not necessary for ribosomal protein S6
683 phosphorylation, increased protein synthesis, or germinal vesicle breakdown in Xenopus
684 oocytes. *Dev. Biol.* **107**, 460–469 (1985).
685 60. Sellier, C. *et al.* Intracellular acidification delays hormonal G2/M transition and inhibits G2/M
686 transition triggered by thiophosphorylated MAPK in Xenopus oocytes. *J. Cell Biochem.* **98,** 287–300
687 (2006).
688 61. Tachibana, K., Machida, T., Nomura, Y. & Kishimoto, T. MAP kinase links the fertilization
689 signal transduction pathway to the G1/S-phase transition in starfish eggs. *EMBO J.* **16**, 4333–4339
690 (1997).
691 62. Tachibana, K., Tanaka, D., Isobe, T. & Kishimoto, T. c-Mos forces the mitotic cell cycle to
692 undergo meiosis II to produce haploid gametes. *Proc. Natl. Acad. Sci. USA* **97**, 14301-14306 (2000).

693 63. Flament, S., Browaeys, E., Rodeau, J. L., Bertout, M. & Vilain, J. P. Xenopus oocyte
694 maturation: cytoplasm alkalization is involved in germinal vesicle migration. *Int. J. Dev.*
695 *Biol.* **40**, 471–476 (1996).
696 64. Kishimoto, T. Microinjection and cytoplasmic transfer in starfish oocytes. *Methods Cell Biol.*
697 **27**, 379-394 (1986).
698 65. Chiba, K. *et al.* The primary structure of the α subunit of a starfish guanosine-nucleotide-
699 binding regulatory protein involved in 1-methyladenine-induced oocyte maturation. *Eur. J.*
700 *Biochem.* **207**, 833–838 (1992).
701 66. Hamaguchi, M., Watanabe, K. & Hamaguchi, Y. Regulation of intracellular pH in sea urchin
702 eggs by medium containing both weak acid and base. *Cell Struct. Funct.* **22**, 387–398 (1997).
703 67. Hijikata, A., Yura, K., Noguti, T. & Go, M. Revisiting gap locations in amino acid sequence
704 alignments and a proposal for a method to improve them by introducing solvent
705 accessibility. *Proteins* **79**, 1868–1877 (2011).

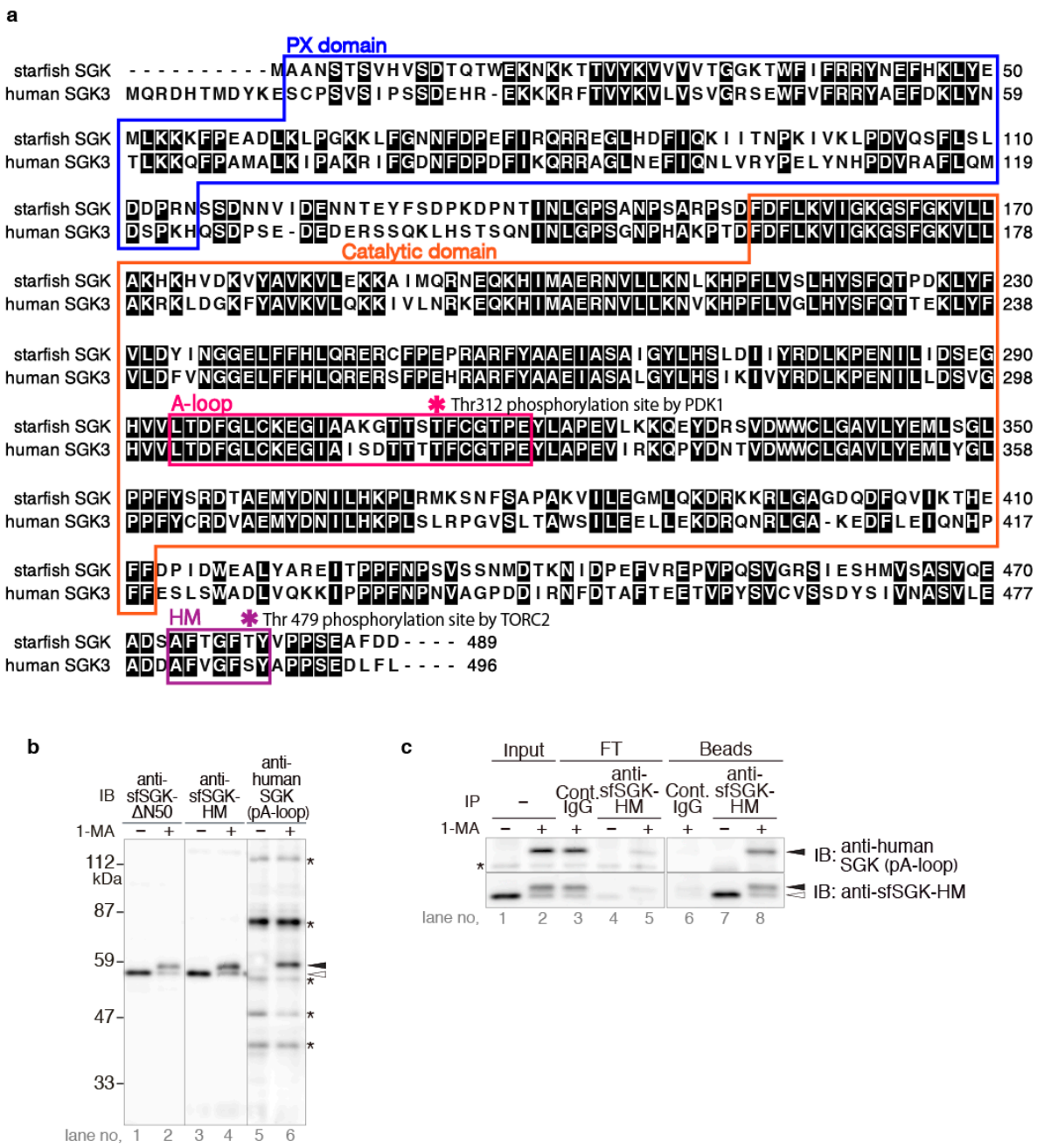

Figure 1 sfSGK protein and phosphorylation of its A-loop are detectable in starfish oocytes.

a The deduced amino acid sequence of starfish SGK (sfSGK) was aligned with that of human SGK3 (NCBI accession number NP_001028750.1) using the ALAdeGAP alignment software[67]. The sfSGK sequence has been submitted to the DDBJ/EMBL/Gen Bank databases under accession number LC430700. Identical amino acids are shaded. Dashes indicate gaps introduced for optimal alignment. Colored boxes indicate conserved domains: PX domain (blue), Activation-loop (A-loop; magenta), Hydrophobic motif (HM; purple), and Catalytic domain (orange). Magenta and purple asterisk indicate conserved residues phosphorylated by PDK1 (Thr312 in starfish; Thr320 in human) and TORC2 (Thr479 in starfish: Ser486 in human), respectively. **b** Unstimulated starfish oocytes were incubated with or without 1-MA for 4 min, followed by immunoblotting with anti-sfSGK-ΔN50,

717 anti-sfSGK-HM, and anti-human phospho-SGK (anti-human SGK [pA-loop]) antibodies. Asterisks
718 indicate non-specific bands. The result shown is representative of three independent experiments. **c**
719 Immunoprecipitation (IP) was performed with anti-sfSGK-HM antibody or control IgG using
720 extracts prepared from unstimulated or 1-MA stimulated oocytes. Input extract (Input), flow-through
721 (FT), and beads (Beads) samples were analyzed by immunoblotting with the indicated antibodies
722 (IB). Asterisk indicates non-specific bands detected by anti-human phospho-SGK (anti-human SGK
723 [pA-loop]). The indicated result is representative of two independent experiments. Closed and open
724 arrowheads indicate positions of the upper and lower bands of sfSGK, respectively (**b**, **c**).

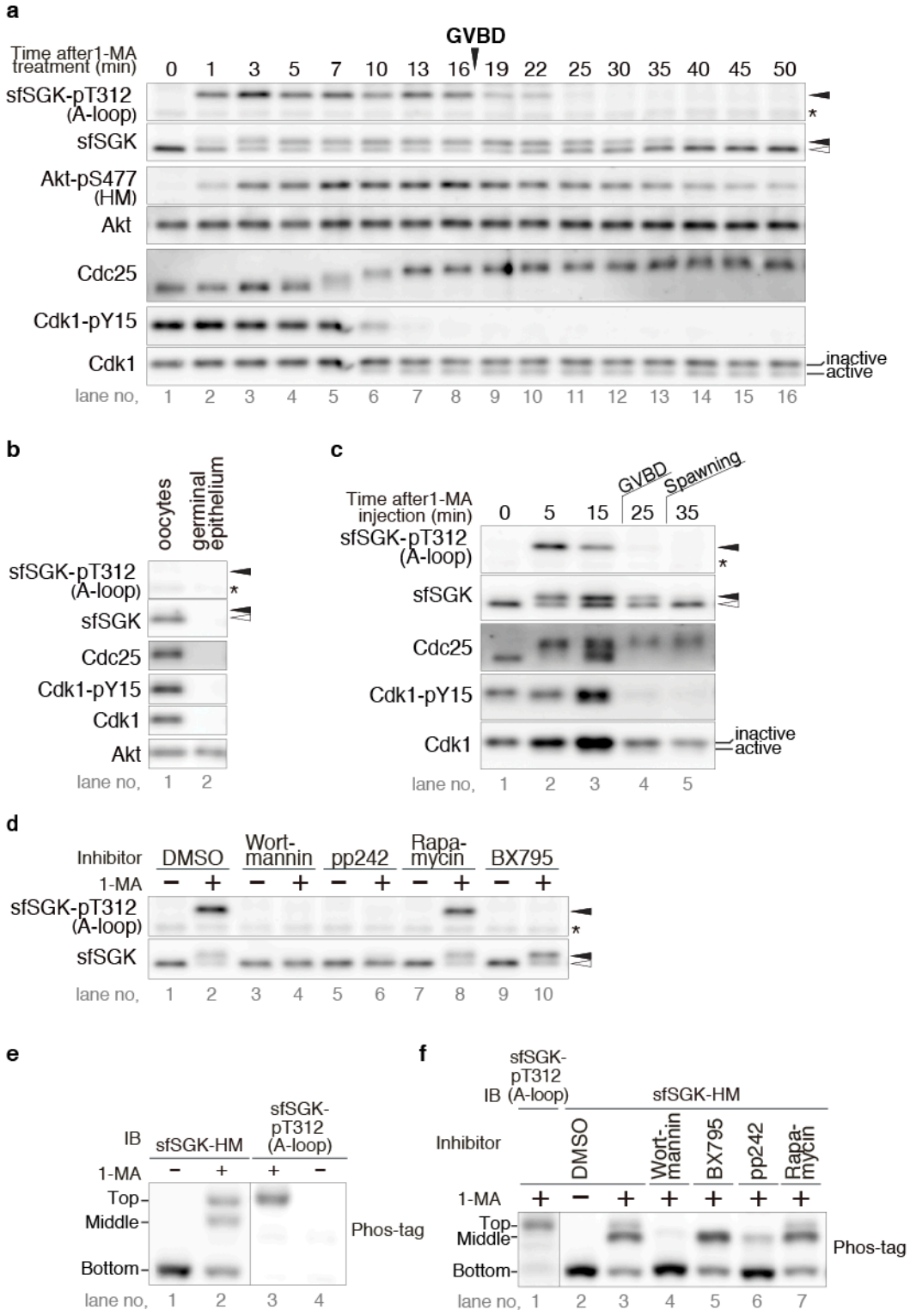

725

726 **Figure 2 sfSGK is activated by PDK1 and TORC2 in a PI3K-dependent manner.**

727 **a** Isolated oocytes were treated with 1-MA and recovered at the indicated times, followed by
728 immunoblotting with anti-human phospho-SGK (sfSGK-pT312 [A-loop]), anti-sfSGK-HM (sfSGK),
729 anti-starfish phospho-Akt-HM (Akt-pS477[HM]), anti-starfish Akt C-terminal fragment (Akt),

730 anti-starfish Cdc25 (Cdc25), anti-phospho-Cdk1 (Cdk1-pY15), and anti-PSTAIR (Cdk1) antibodies.
731 GVBD occurred at 17 min. The result shown is representative of three independent experiments. **b** A
732 piece of ovary was taken from female starfish, separated into oocytes and germinal epithelium, and
733 subjected to immunoblotting with indicated antibodies. **c** To stimulate ovarian oocytes, 1-MA was
734 injected into the body cavity of female starfish, and then two pieces of ovaries were recovered at
735 indicated times. One piece of ovary was immediately added to sample buffer for immunoblotting
736 with the indicated antibodies. Oocytes from the other piece of the ovary were monitored to count
737 GVBD. GVBD occurred within 25 min, and spawning started at 30 min. The result shown is
738 representative of two independent experiments. **d** Isolated oocytes were treated with 1-MA for 4 min
739 in the presence of indicated inhibitors or DMSO, and then subjected to normal SDS-PAGE, followed
740 by immunoblotting with the indicated antibodies. The result shown is representative of two
741 independent experiments. **e** Isolated oocytes were treated with 1-MA for 4 min, and then subjected to
742 Phos-tag SDS-PAGE, followed by immunoblotting with the indicated antibodies (IB). The result
743 shown is representative of three independent experiments. **f** Isolated oocytes were treated with 1-MA
744 for 4 min in the presence of indicated inhibitors, and subjected to Phos-tag SDS PAGE, followed by
745 immunoblotting with the indicated antibodies (IB). The result shown is representative of three
746 independent experiments. Closed and open arrowheads indicate positions of the upper and lower
747 band of sfSGK, respectively (**a**, **b, c** and **d**). Asterisks indicate non-specific bands (**a**, **b**, **c,** and **d**).

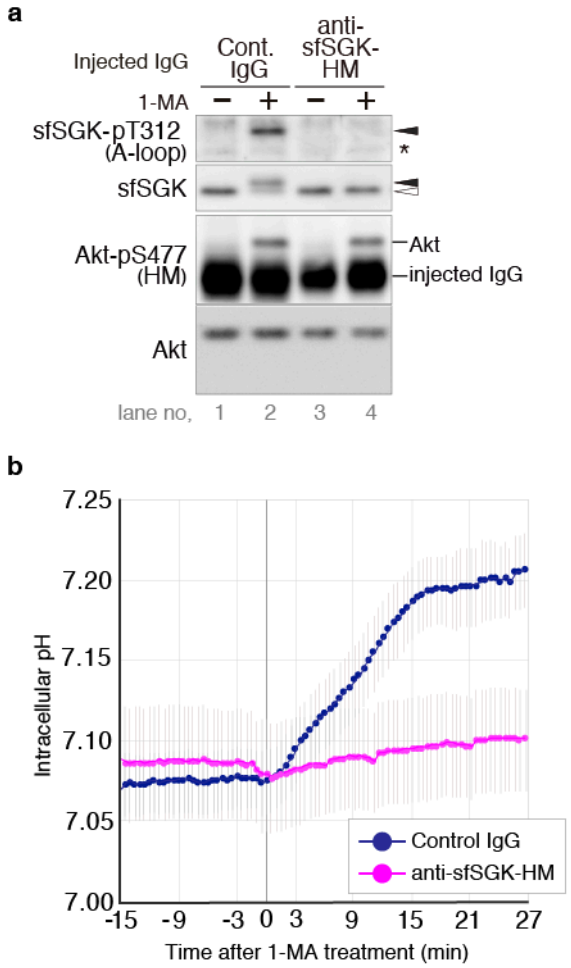

Figure 3 Activation of sfSGK is required for rapid pH_i increase after 1-MA stimulus.

a Unstimulated oocytes were injected with an anti-sfSGK-HM antibody or control IgG, treated with 1-MA for 4 min, and then subjected to immunoblotting with indicated antibodies. Asterisk indicates non-specific bands. Closed and open arrowheads indicate positions of the upper and lower band of sfSGK, respectively. The result shown is representative of three independent experiments. **b** BCECF-dextran and either anti-sfSGK-HM antibody or control IgG were co-injected into unstimulated oocytes. After a 1-h incubation, 1-MA was added, and the fluorescence intensity ratio was measured every 30 seconds before and after 1-MA addition. pH_i was calculated from the fluorescence intensity ratio and plotted. Data represent means ± SE of three independent experiments.

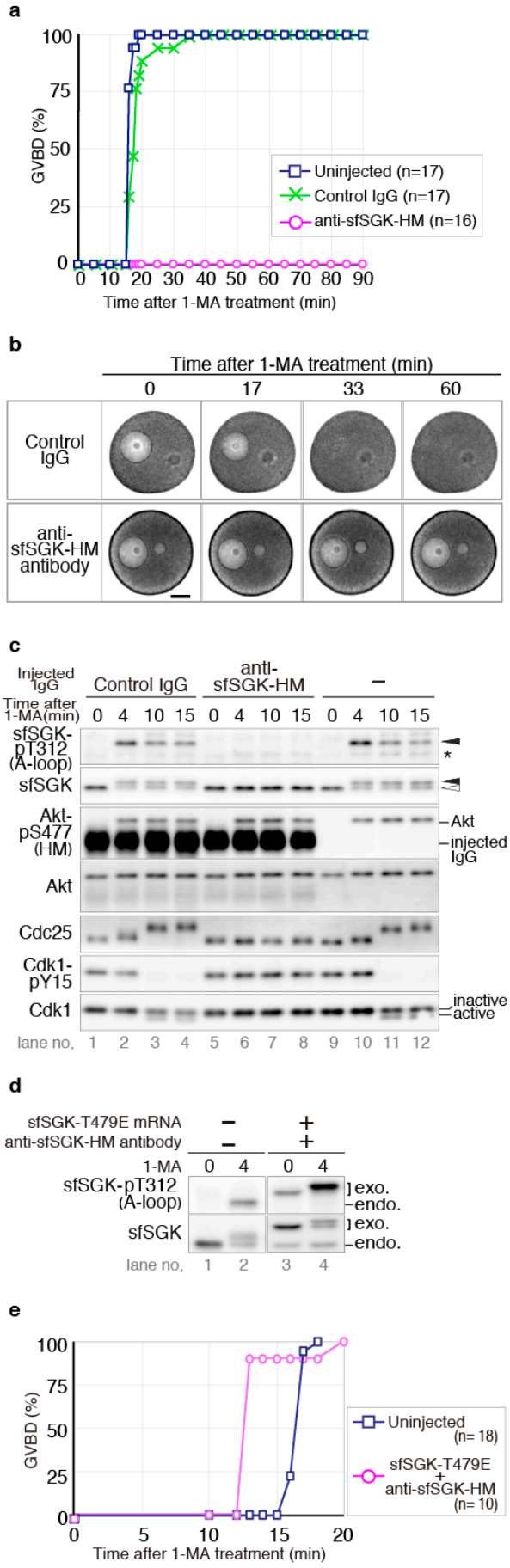
a
GVBD (%)
Time after 1-MA treatment (min)
Uninjected (n=17)
Control IgG (n=17)
anti-sfSGK-HM (n=16)
b
Time after 1-MA treatment (min)
Control IgG
anti-sfSGK-HM antibody
c
Injected IgG
Control IgG
anti-sfSGK-HM
Time after 1-MA(min)
sfSGK-pT312 (A-loop)
sfSGK
Akt-pS477 (HM)
Akt
Cdc25
Cdk1-pY15
Cdk1
Akt
injected IgG
inactive
active
lane no,
d
sfSGK-T479E mRNA
anti-sfSGK-HM antibody
1-MA
sfSGK-pT312 (A-loop)
sfSGK
exo.
endo.
lane no,
e
GVBD (%)
Time after 1-MA treatment (min)
Uninjected (n= 18)
sfSGK-T479E + anti-sfSGK-HM (n= 10)

759

760 **Figure 4 Activation of sfSGK is required for cyclin B–Cdk1 activation.**

761 **a–c** Unstimulated oocytes were injected with anti-sfSGK-HM antibody or control IgG, treated with
762 1-MA, and subjected to the following experiments: monitoring of GVBD (**a**), imaging by differential
763 interference contrast (DIC) microscopy (**b**), and immunoblotting with the indicated antibodies (**c**) at
764 the indicated times. "n" indicates the number of oocytes observed (**a**). An oil drop, that had been
765 introduced along with the antibodies as a mark of the microinjection, was observed on the right of
766 the GV (**b**). Scale bar represents 50 μm (**b**). Asterisk indicates a non-specific band (**c**). Closed and
767 open arrowheads indicate positions of the upper band and the lower band of sfSGK, respectively (**c**).
768 Results are representative of two independent experiments. **d**, **e** Anti-sfSGK-HM antibody was
769 injected into unstimulated oocytes. After incubation for 1 h, mRNA encoding a mutant sfSGK
770 (T479E) was injected into the same oocytes, followed by incubation for 17 h. As a control,
771 uninjected oocytes were incubated for 17 h. These oocytes were treated with 1-MA, followed by
772 immunoblotting with indicated antibodies (**d**) and counting of GVBD (**e**) at the indicated times. "exo."
773 and "endo." indicate exogenous and endogenous sfSGK, respectively (**d**). "n" indicates the number
774 of oocytes observed (**e**). Results are representative of two independent experiments.

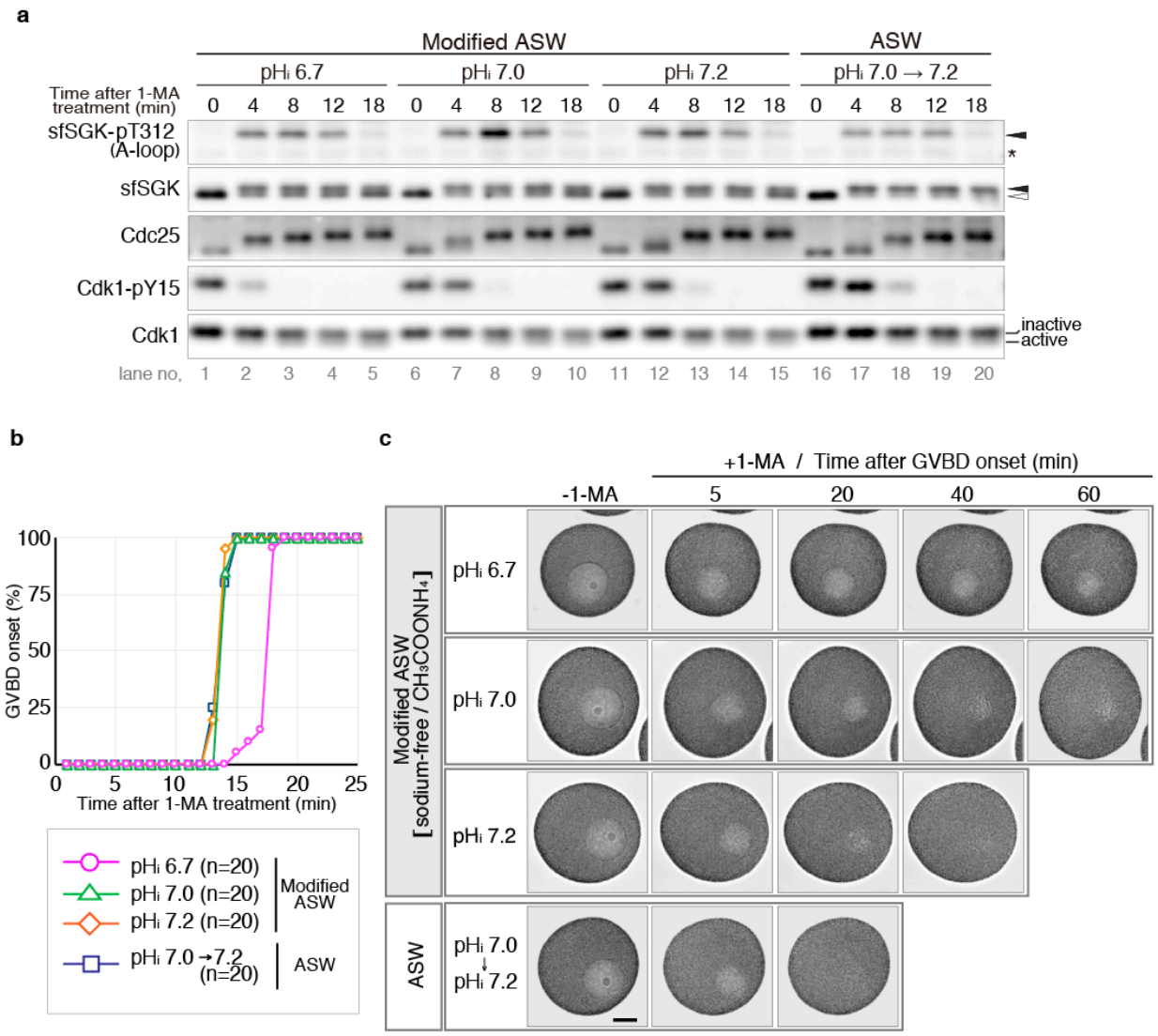

Figure 5 Reduced pH_i delays onset of GVBD and blocks completion of GVBD without affecting cyclin B–Cdk1 activation.

a To clamp pH_i at 6.7, 7.0, and 7.2, unstimulated oocytes were incubated with sodium-free artificial seawater containing CH_3COONH_4 (Modified ASW) for 20 min. As a control, unstimulated oocytes were incubated in artificial seawater (ASW) for 20 min, in which pH_i is approximately 7.0, and increases to ~7.2 after 1-MA treatment[17] (see also control IgG–injected oocytes in Fig. 3b). These oocytes were treated with 1-MA and analyzed by immunoblotting with indicated antibodies. Asterisk indicates a non-specific band. Closed and open arrowheads indicate the positions of the upper and lower bands of sfSGK, respectively. **b** Oocytes treated as described in **a** were monitored to count onset of GVBD. "n" indicates the number of oocytes observed. Morphology of GVBD onset is shown in Supplementary Fig. 2. **c** Time-lapse DIC images of oocytes treated as described in **a** were taken every 10 seconds before and after addition of 1-MA. Images at selected times after GVBD onset are shown. Scale bar represents 50 µm. For complete image sequences, see Supplementary movies 1–4. For Z-stack images acquired after the time-lapse imaging, see Supplementary Fig. 3. Results in all panels are representative of two independent experiments.

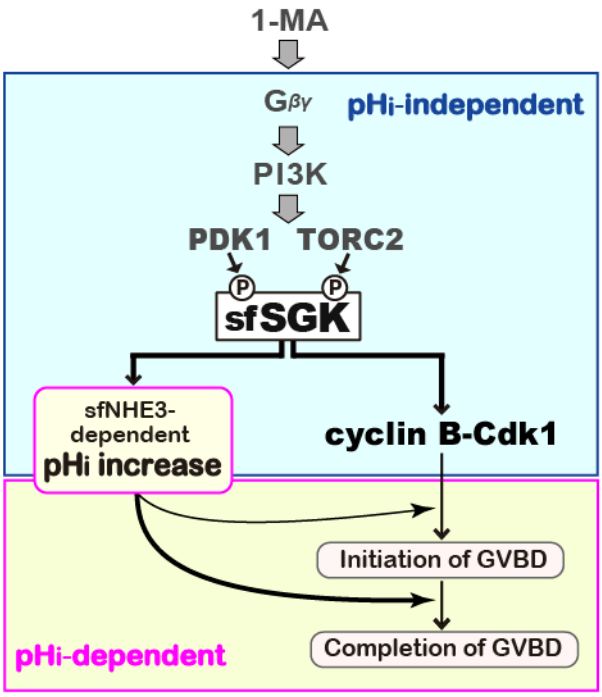

Figure 6 Model for sfSGK-dependent meiotic resumption: sfSGK induces cyclin B–Cdk1 activation to resume meiosis and pH_i increase to complete GVBD in ovarian oocytes.
A model for 1-MA–induced meiotic resumption in ovarian oocytes was prepared on the basis of previous and current findings. 1-MA stimulus induces the release of Gβγ from Gαi, leading to PI3K activation. In a manner that depends on PI3K, sfSGK is activated via phosphorylation of the A-loop by PDK1 after prior phosphorylation of the HM by TORC2. Activation of sfSGK is essential for cyclin B–Cdk1 activation and sfNHE3-dependent pH_i increase. These SGK-dependent pathways are pH_i-independent (blue box). On the other hand, time to GVBD onset after cyclin B–Cdk1 activation and completion of GVBD are pH_i-dependent (yellow box), and both are defective at pH_i of 6.7. Because pH_i of ovarian oocytes before 1-MA stimulation in body cavity is ~6.7, the sfSGK-dependent pH_i increase after 1-MA stimulus accelerates GVBD onset and is required for completion of GVBD in ovarian oocytes. By contrast, the pH_i of isolated oocytes before 1-MA stimulation in ASW is ~7.0, which is already permissive for GVBD. Therefore, a pH_i increase is not essential for GVBD in isolated oocytes.